A&A 543, A144 (2012)
DOI: 10.1051/0004-6361/201219193

Astronomy & Astrophysics

Atomic data for astrophysics: Fe XIII soft X-ray lines*

G. Del Zanna[1] and P. J. Storey[2]

[1] DAMTP, Centre for Mathematical Sciences, Wilberforce Road, Cambridge, CB3 0WA, UK
e-mail: g.del-zanna@damtp.cam.ac.uk
[2] Department of Physics and Astronomy, University College London, Gower Street, London, WC1E 6BT, UK

Received 8 March 2012 / Accepted 14 May 2012

ABSTRACT

We present new large-scale R-matrix (up to $n = 4$) and distorted wave (up to $n = 6$) scattering calculations for electron collisional excitation of Fe XIII. We aim to provide accurate atomic data for the soft X-rays, where strong $n = 4 \rightarrow n = 3$ transitions are present. As found in previous work on Fe X, resonances from within the $n = 4$ levels and cascading from higher levels significantly increase the intensities of these lines. We provide a number of models and line intensities, and list a number of strong unidentified lines.

Key words. atomic data – line: identification – Sun: corona – techniques: spectroscopic

1. Introduction

The soft X-ray (50–170 Å) spectrum of the quiet and active Sun is rich in $n = 4 \rightarrow n = 3$ transitions from highly ionised iron ions, from Fe VII to Fe XVI (see, e.g. Fawcett et al. 1968; Manson 1972; and Behring et al. 1976). Very little atomic data are currently available for these ions and the majority of the spectral lines still await firm identification, despite the fact that various instruments are routinely observing the soft X-rays, such as the Atmospheric Imaging Assembly (AIA, see Lemen et al. 2012) and the Extreme ultraviolet Variability Experiment (EVE; Woods et al. 2012) on-board the Solar Dynamic Observatory (SDO), and the *Chandra* Low Energy Transmission Grating spectrometer (LETG, see Brinkman et al. 2000).

New atomic data for Fe VIII and Fe IX relevant for the soft X-rays have been presented in O'Dwyer et al. (2012). Rather unexpectedly, these authors found substantial enhancements of the excitation rates from the ground levels to some of the levels of the $n = 4$ configurations due to resonances converging on other $n = 4$ levels. The same effects were seen by Del Zanna et al. (2012a) for Fe X and Del Zanna et al. (2012b) for Fe XII. Here, we present new large-scale scattering calculations for the Fe XIII soft X-ray lines.

This paper is organised as follows. In Sect. 2, we give a brief review of previous observations and atomic calculations. In Sect. 3 we outline the methods we adopted for the scattering calculations. In Sect. 4 we present our results and in Sect. 5 we reach our conclusions.

2. Previous observations and atomic data for Fe XIII

A complete review of the Fe XIII line identifications and wavelengths for the $n = 3$ levels is given in Del Zanna (2011), where a number of new energy levels were identified. These new energies, derived from observation are adopted here.

The identifications of some of the $3s^2 3p^2\ 4l$ (l = s, p, d, f) levels are due to the fundamental laboratory work by Fawcett et al. (1972), from laboratory spectra in the soft X-rays of $n = 4 \rightarrow n = 3$ transitions. A few transitions were only tentatively identified, and the spectra contain a large number of unidentified lines. We have re-analysed some of Fawcett's plates as part of a larger project to complete the identification work on the Fe soft X-ray spectrum.

After Fawcett et al. (1972), Kastner et al. (1978) provided some tentative identifications of a few further lines. Vilkas & Ishikawa (2004) later reviewed the above identifications based on ab-initio atomic structure calculations, suggesting that in several cases misidentifications have occurred for cases when large differences between ab-initio and experimental energies were present.

There are a number of atomic data calculations for the $n = 3$ levels, reviewed in the Iron Project work of Storey & Zeippen (2010, hereafter SZ10). SZ10 performed an R-matrix calculation for the lowest 54 *LS* terms and 114 fine-structure levels within the $n = 3$ complex. eleven $n = 3$ configurations were included in the expansion of the target wavefunctions.

The SZ10 atomic data were benchmarked against well-calibrated observations in Del Zanna (2011, 2012). Excellent agreement, within a few percent, was found between most predicted and observed line intensities. To our knowledge, the present are the first R-matrix calculations for the $n = 4$ levels.

3. Methods

The atomic structure calculations were carried out using the AUTOSTRUCTURE program (Badnell 1997) which constructs target wavefunctions using radial wavefunctions calculated in a scaled Thomas-Fermi-Dirac statistical model potential with a set of scaling parameters.

The Breit-Pauli distorted wave (DW) calculations were carried out using the recent development of the AUTOSTRUCTURE

* The full dataset (energies, transition probabilities and rates) are available in electronic form at our APAP website (http://www.apap-network.org) as well as at the CDS via anonymous ftp to cdsarc.u-strasbg.fr (130.79.128.5) or via http://cdsarc.u-strasbg.fr/viz-bin/qcat?J/A+A/543/A144

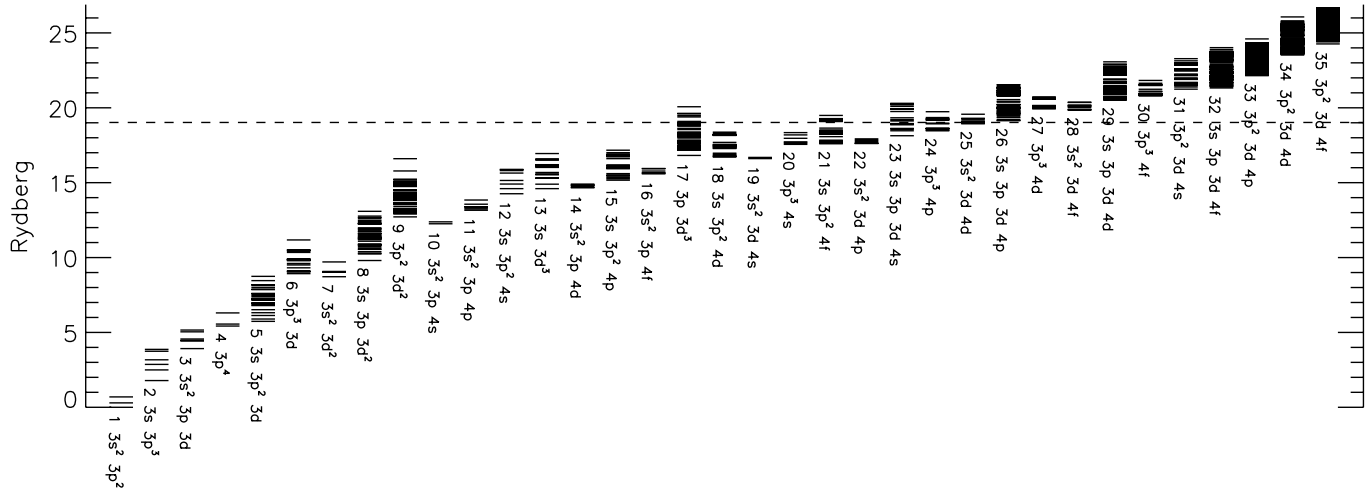

Fig. 1. Term energies of the target levels (35 configurations) for the $n = 4$ calculations. The 331 terms within the lowest 25 configurations which produce levels having energies below the dashed line have been retained for the close-coupling expansion.

code, described in detail in Badnell (2011). Collision strengths are calculated at the same set of final scattered energies for all transitions. "Top-up" for the contribution of high partial waves is done using the same Breit-Pauli methods and subroutines implemented in the R-matrix outer-region code STGF. The program also provides radiative rates and infinite energy Born limits. These limits are particularly important for two reasons. First, they allow a consistency check of the collision strengths in the scaled Burgess & Tully (1992) domain (see also Burgess et al. 1997). Second, they are used in the interpolation of the collision strengths at high energies when calculating the Maxwellian averages.

The R-matrix method used in the inner region of the scattering calculation is described in Hummer et al. (1993) and Berrington et al. (1995). We performed the calculation in *LS* coupling and included the mass-velocity and Darwin relativistic operators. The outer region calculation used the intermediate-coupling frame transformation (ICFT) method (Griffin et al. 1998). Dipole-allowed transitions were topped-up to infinite partial wave using an intermediate coupling version of the Coulomb-Bethe method as described by Burgess (1974) while non-dipole allowed transitions were topped-up assuming that the collision strengths form a geometric progression in J (see Badnell & Griffin 2001). The collision strengths were extended to high energies by interpolation using the appropriate high-energy limits in the Burgess & Tully (1992) scaled domain. The high-energy limits were calculated with AUTOSTRUCTURE for both optically-allowed (see Burgess et al. 1997) and non-dipole allowed transitions (see Chidichimo et al. 2003). The temperature-dependent effective collisions strength $\Upsilon(i-j)$ were calculated by assuming a Maxwellian electron distribution and linear integration with the final energy of the colliding electron.

4. Results

4.1. Distorted wave calculations

We performed various DW calculations systematically increasing the number of configurations up to and including those with $n = 6$ valence orbitals. The DW rates for the higher levels were initially supplemented with the SZ10 atomic data, to ensure that the metastable levels are correctly populated.

We then carried out separate structure calculations for each ion model to calculate all of the radiative data for all transitions among the levels. This ensures that all the cascading from the target configurations is included. We then calculated the level populations and the relative line intensities so as to find out which lines are expected to be strongest. These results were then compared to the laboratory plates of B.C. Fawcett and to solar spectra.

As in the Fe x case (Del Zanna et al. 2012a), we found that many lines were predicted which so far have not been identified in any spectra and many discrepancies between observed and predicted intensities. We then followed the procedure outlined in the Fe x case to estimate which configurations would be likely to be producing resonances in the collision strengths for the spectroscopically important configurations and levels. The final R-matrix scattering calculation was constructed so as to include those configurations which were found to be most likely to cause significant resonant enhancements to the spectroscopically important $n = 4$ levels. For Fe XIII, we found that the excitations to the $3s^2$ 3p 4s levels are significantly underestimated by the DW calculations, mostly because of resonances due to the $3s^2$ 3p 4p levels.

4.2. The R-matrix and DW calculations for the n = 3, 4 levels

As our configuration basis set we have chosen the complete $n = 3, 4$ set of 35 configurations shown in Fig. 1 and listed in Table 1. The scaling parameters λ_{nl} for the potentials in which the orbital functions are calculated are also given in Table 1. A full R-matrix calculation with all the $n = 4$ levels is currently prohibitive, because it would involve 944 *LS* terms and 2186 levels. For the scattering close-coupling calculation, we retained 749 fine-structure levels arising from the first 331 *LS* terms of the lowest set of 25 configurations (see Fig. 1). We have performed both an ICFT R-matrix (RM4) and a DW calculation (DW4) using the same basis.

Tables 2, 3 present a selection of fine-structure target level energies E_t, compared to experimental energies E_{exp}. The latter have been obtained from Del Zanna (2011) for the $n = 3$ levels, otherwise from a selection of identifications which we assessed.

There is good overall agreement in terms of energy differences between levels. A set of "best" energies E_b was obtained

Table 1. Target electron configuration basis and orbital scaling parameters λ_{nl} for the R-matrix and DW runs.

Configurations		λ_{nl}
$3s^2\ 3p^2$	1s	1.40878
$3s^2\ 3p\ 3d$	2s	1.11326
$3s^2\ 3p\ 3d^2$	2p	1.05795
$3s^2\ 3p\ 4l$ (l = s, p, d, f)	3s	1.12011
$3s^2\ 3d\ 4l$ (l = s, p, d, f)	3p	1.08939
$3s^2\ 3d^2$	3d	1.10792
$3s\ 3p^3$	4s	1.14323
$3s\ 3p^2\ 3d$	4p	1.11142
$3s\ 3p^2\ 4l$ (l = s, p, d, f)	4d	1.13622
$3s\ 3p\ 3d^2$	4f	1.28399
$3s\ 3p\ 3d\ 4l$ (l = s, p, d, f)	5s	1.13910
$3s\ 3d^3$	5p	1.10732
$3p^4$	5d	1.13470
$3p^3\ 3d$	5f	1.26407
$3p^3\ 4l$ (l = s, p, d, f)	5g	1.40504
$3p^2\ 3d^2$	6s	1.14928
$3p^2\ 3d\ 4l$ (l = s, p, d, f)	6p	1.11694
$3p\ 3d^3$	6d	1.14512
$3s^2\ 3p\ 5l$ (l = s, p, d, f, g)	6f	1.27387
$3s\ 3p^2\ 5l$ (l = s, p, d, f, g)	6g	1.41023
$3p^3\ 5l$ (l = s, p, d, f, g)		
$3s^2\ 3p\ 6l$ (l = s, p, d, f, g)		
$3s\ 3p^2\ 6l$ (l = s, p, d, f, g)		
$3p^3\ 6l$ (l = s, p, d, f, g)		

Notes. The configurations above the line were used for the RM4 and DW4 calculations. Those below the line were used for the DW calculation DW6.

with a quadratic fit between the E_{exp} and E_t values. The E_b values were used (together with the E_{exp} ones) within the R-matrix calculation to obtain an accurate position of the resonance thresholds. They were also used to calculate the transition probabilities, which was done separately.

Table 2 also shows the energies of the SZ10 target basis for the $n = 3$ levels. The energies are very close, indeed for the $n = 3$ levels the present target is very similar to the SZ10 one. Table 3 also shows the values calculated by Vilkas & Ishikawa (2004) for the $n = 4$ levels. Good agreement with the experimental energies is present.

The expansion of each scattered electron partial wave was done over a basis of 18 functions within the R-matrix boundary and the partial wave expansion extended to a maximum total orbital angular momentum quantum number of $L = 16$. This produces reliable collision strengths up to about 80 Ryd.

The outer region calculation includes exchange up to a total angular momentum quantum number $J = 27/2$. We have supplemented the exchange contributions with a non-exchange calculation extending from $J = 29/2$ to $J = 75/2$. The outer region exchange calculation was performed in a number of stages. A coarse energy mesh was chosen above all resonances. The resonance region itself was calculated with 6800 points.

We then compared the thermally-averaged collision strengths with the R-matrix results by SZ10 for the $n = 3$ levels. Excellent agreement is found.

As an example, Fig. 2 shows a comparison between the present thermally-averaged collision strengths at 40 and 1 MK, compared to those of SZ10, for all transitions between the ground configuration levels and those up to level 27 (i.e. all among $3s^2\ 3p^2$ and between $3s^2\ 3p^2$ and $3s\ 3p^3$, $3s^2\ 3p\ 3d$). Excellent agreement, to within a few percent, is found at higher temperatures and at low temperatures for all the strongest transitions. For the weaker ones, the present collision strengths are slightly higher at low temperatures, indicating some resonance enhancement due to the larger target.

We also compared the intensities for the brightest lines as obtained with the SZ10 and the present rates, and found the same numbers, within a few percent, at the temperature of maximum ion abundance in ionization equilibrium ($\log T_e$ [K] = 6.25).

Table 2. Level energies for Fe XIII ($n = 3$).

i	Conf.	Lev.	E_{exp}	E_t	E_t (SZ10)
1	$3s^2\ 3p^2$	$^3P_0$	0.0	0.0	0.0
2	$3s^2\ 3p^2$	$^3P_1$	0.085	0.081 (0.003)	0.081 (0.004)
3	$3s^2\ 3p^2$	$^3P_2$	0.169	0.167 (0.002)	0.166 (0.003)
4	$3s^2\ 3p^2$	$^1D_2$	0.438	0.451 (–0.013)	0.452 (–0.014)
5	$3s^2\ 3p^2$	$^1S_0$	0.834	0.858 (–0.024)	0.851 (–0.017)
6	$3s\ 3p^3$	$^5S_2$	1.956	1.911 (0.044)	1.914 (0.041)
7	$3s\ 3p^3$	$^3D_1$	2.617	2.608 (0.009)	2.610 (0.007)
8	$3s\ 3p^3$	$^3D_2$	2.619	2.610 (0.009)	2.611 (0.008)
9	$3s\ 3p^3$	$^3D_3$	2.644	2.635 (0.009)	2.636 (0.008)
10	$3s\ 3p^3$	$^3P_0$	2.997	3.001 (–0.004)	2.997 (0.001)
11	$3s\ 3p^3$	$^3P_1$	3.004	3.008 (–0.004)	3.003 (0.001)
12	$3s\ 3p^3$	$^3P_2$	3.010	3.013 (–0.003)	3.008 (0.002)
13	$3s\ 3p^3$	$^1D_2$	3.302	3.320 (–0.017)	3.319 (–0.017)
14	$3s\ 3p^3$	$^3S_1$	3.786	3.839 (–0.053)	3.833 (–0.047)
15	$3s^2\ 3p\ 3d$	$^3F_2$	3.920	3.968 (–0.049)	3.972 (–0.053)
16	$3s^2\ 3p\ 3d$	$^3F_3$	3.981	4.031 (–0.049)	4.034 (–0.052)
17	$3s\ 3p^3$	$^1P_1$	3.992	4.049 (–0.057)	4.045 (–0.053)
18	$3s^2\ 3p\ 3d$	$^3F_4$	4.073	4.121 (–0.048)	4.123 (–0.050)
19	$3s^2\ 3p\ 3d$	$^3P_2$	4.432	4.507 (–0.075)	4.505 (–0.073)
20	$3s^2\ 3p\ 3d$	$^3P_1$	4.510	4.580 (–0.070)	4.579 (–0.069)
21	$3s^2\ 3p\ 3d$	$^1D_2$	4.546	4.619 (–0.073)	4.617 (–0.071)
22	$3s^2\ 3p\ 3d$	$^3P_0$	4.570	4.632 (–0.061)	4.630 (–0.059)
23	$3s^2\ 3p\ 3d$	$^3D_1$	4.616	4.687 (–0.071)	4.688 (–0.072)
24	$3s^2\ 3p\ 3d$	$^3D_2$	4.641	4.715 (–0.075)	4.716 (–0.076)
25	$3s^2\ 3p\ 3d$	$^3D_3$	4.640	4.719 (–0.079)	4.721 (–0.081)
26	$3s^2\ 3p\ 3d$	$^1F_3$	5.075	5.180 (–0.105)	5.179 (–0.104)
27	$3s^2\ 3p\ 3d$	$^1P_1$	5.201	5.305 (–0.104)	5.302 (–0.101)
28	$3p^4$	$^3P_2$	5.389	5.492 (–0.103)	5.490 (–0.101)
29	$3p^4$	$^3P_1$	–	5.604	5.602
30	$3p^4$	$^3P_0$	–	5.631	5.629
31	$3p^4$	$^1D_2$	–	5.715	5.709
32	$3s\ 3p^2\ 3d$	$^5F_1$	–	5.776	5.781
33	$3s\ 3p^2\ 3d$	$^5F_2$	–	5.797	5.801
34	$3s\ 3p^2\ 3d$	$^5F_3$	–	5.829	5.833
35	$3s\ 3p^2\ 3d$	$^5F_4$	–	5.875	5.879
36	$3s\ 3p^2\ 3d$	$^5F_5$	–	5.934	5.938
37	$3s\ 3p^2\ 3d$	$^5D_0$	–	5.985	5.986
38	$3s\ 3p^2\ 3d$	$^5D_1$	–	5.992	5.992
39	$3s\ 3p^2\ 3d$	$^5D_2$	–	6.003	6.004
40	$3s\ 3p^2\ 3d$	$^5D_3$	–	6.020	6.020
41	$3s\ 3p^2\ 3d$	$^5D_4$	–	6.046	6.046
42	$3s\ 3p^2\ 3d$	$^3F_2$	6.102	6.217 (–0.116)	6.220 (–0.118)
56	$3s\ 3p^2\ 3d$	$^3D_2$	6.869	6.991 (–0.122)	6.989 (–0.120)
60	$3s\ 3p^2\ 3d$	$^3F_2$	7.089	7.217 (–0.128)	7.217 (–0.128)
61	$3s\ 3p^2\ 3d$	$^3F_3$	7.140	7.268 (–0.128)	7.268 (–0.128)
65	$3s\ 3p^2\ 3d$	$^3F_4$	7.218	7.346 (–0.128)	7.346 (–0.127)
72	$3s\ 3p^2\ 3d$	$^3D_2$	7.447	7.580 (–0.133)	7.582 (–0.135)
84	$3s\ 3p^2\ 3d$	$^3P_2$	8.179	8.311 (–0.133)	–

Notes. The experimental level energies E_{exp} (in Rydbergs, from Del Zanna 2011 for the $n = 3$) are shown, together with those obtained from our scattering target E_t and those from the scattering calculation of SZ10. Values in parentheses indicate differences with E_{exp}. Only a selection of levels is shown.

Table 3. Level energies for Fe XIII (n = 4).

i	Conf.	Lev.	E_{exp}	E_t	E_t (VI04)
210	$3s^2$ 3p 4s	$^3P_1$	12.177	12.309 (–0.132)	12.175 (0.002)
218	$3s^2$ 3p 4s	$^3P_2$	–	12.440	12.319
221	$3s^2$ 3p 4s	$^1P_1$	12.410	12.535 (–0.125)	12.394 (0.016)
259	$3s^2$ 3p 4p	$^3D_2$	–	13.347	13.402
265	$3s^2$ 3p 4p	$^3P_0$	–	13.435	13.276
267	$3s^2$ 3p 4p	$^3D_3$	–	13.464	13.355
268	$3s^2$ 3p 4p	$^3P_1$	–	13.479	13.216
272	$3s^2$ 3p 4p	$^3P_2$	–	13.547	13.228
282	$3s^2$ 3p 4p	$^1D_2$	13.561	13.714 (–0.153)	13.556 (0.005)
331	3s $3p^2$ 4s	$^3P_0$	–	14.644	14.470
334	3s $3p^2$ 4s	$^3P_1$	–	14.693	14.516
341	$3s^2$ 3p 4d	$^3D_1$	14.615	14.761 (–0.146)	14.610 (0.005)
342	$3s^2$ 3p 4d	$^3D_2$	14.620	14.766 (–0.146)	14.615 (0.005)
343	3s $3p^2$ 4s	$^3P_2$	–	14.770	14.598
344	$3s^2$ 3p 4d	$^3D_3$	14.639	14.787 (–0.147)	14.635 (0.005)
347	$3s^2$ 3p 4d	$^3F_3$	14.759	14.909 (–0.150)	14.770 (–0.011)
355	$3s^2$ 3p 4d	$^1F_3$	14.859	15.001 (–0.142)	14.850 (0.009)
400	$3s^2$ 3p 4f	$^1F_3$	15.519	15.666 (–0.147)	15.499 (0.020)
407	$3s^2$ 3p 4f	$^3G_4$	15.550	15.725 (–0.175)	15.554 (–0.004)
409	$3s^2$ 3p 4f	$^3F_2$	–	15.741	15.565
416	3s $3p^2$ 4s	$^3P_0$	–	15.830	15.623
417	$3s^2$ 3p 4f	$^3F_4$	–	15.843	15.678
418	$3s^2$ 3p 4f	$^3G_5$	15.687	15.846 (–0.159)	15.691 (–0.003)
423	$3s^2$ 3p 4f	$^3D_1$	15.799	15.960 (–0.161)	15.802 (–0.003)
428	$3s^2$ 3p 4f	$^1G_4$	15.888	16.085 (–0.197)	15.892 (–0.004)

Notes. Same as Table 2, but this time the values from the structure calculations of Vilkas & Ishikawa (2004) (VI04) are shown.

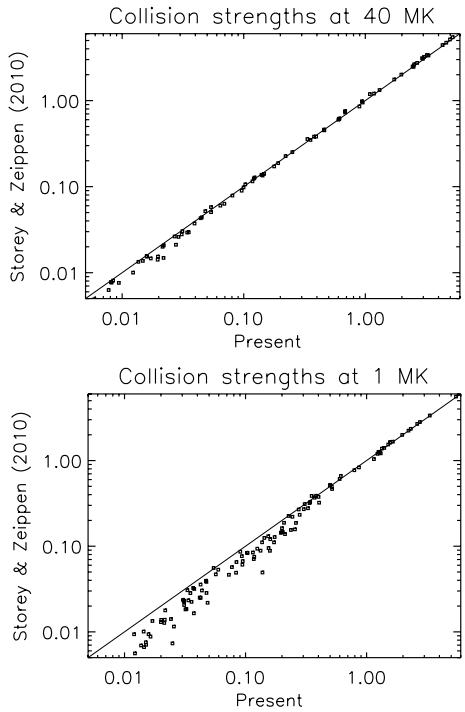

Fig. 2. Thermally-averaged collision strengths (SZ10 vs. the present ones) for a selection of transitions (see text).

4.3. The soft X-ray lines

We have constructed an ion population model (RM4) with the new R-matrix rates, complemented with a set of A-values calculated separately with exactly the same target, but with the experimental and best energies. We did the same with the DW collision strengths, building an ion model (DW4) with the same set of A-values. We then calculated line intensities and looked at how levels are populated at log N_e [cm^{-3}] = 8 and log T_e [K] = 6.25, the temperature of maximum ion abundance in ionization equilibrium. The brightest lines are listed in Table 4.

The comparisons for a selection of n = 4 levels giving rise to some among the strongest transitions are displayed in Figs. 3–6. Excellent agreement between the background R-matrix and the DW collision strengths is found in all cases. This is to be expected since they both use the same target.

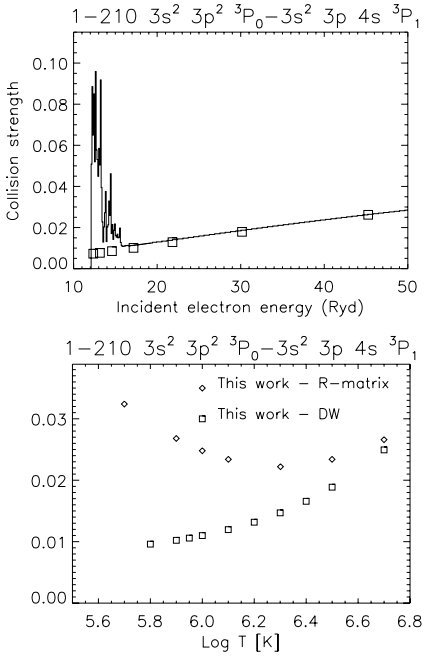

Fig. 3. *Above*: collision strength for the 1–210 transition, averaged over 0.1 Ryd in the resonance region. The data points are displayed in histogram mode. *Below*: thermally-averaged collision strengths. Boxes indicate the DW values.

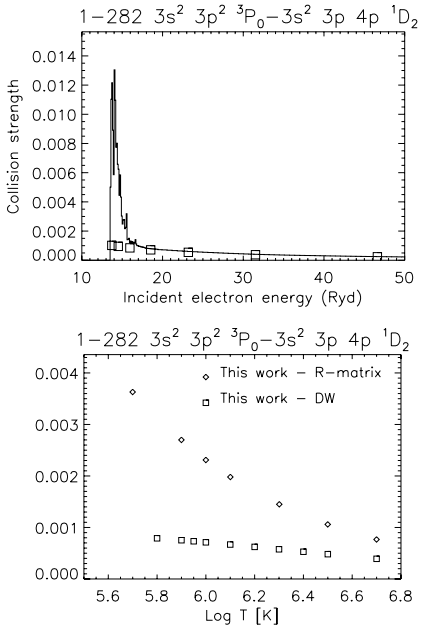

Fig. 4. Same as Fig. 3, for the 1–282 transition.

Table 4. Relative intensities of the brightest Fe XIII lines in the soft X-rays.

i–j	Levels	Int 1.0×10^{8} DW4	Int 1.0×10^{8} RM4	Int 1.0×10^{8} RM4+DW6	Int 1.0×10^{12} RM4	gf	$A_{ji}(s^{-1})$	λ_{exp}(Å)	λ_{th}(Å)
7–331	$3s\ 3p^3\ ^3D_1$–$3s\ 3p^2\ 4s\ ^3P_0$	1.6×10^{-2}	1.6×10^{-2}	1.6×10^{-2}	1.6×10^{-3}	0.12	1.4×10^{11}	–	75.71
7–265	$3s\ 3p^3\ ^3D_1$–$3s^2\ 3p\ 4p\ ^3P_0$	1.1×10^{-2}	1.1×10^{-2}	1.1×10^{-2}	1.2×10^{-3}	3.2×10^{-2}	3.0×10^{10}	–	84.17
20–409	$3s^2\ 3p\ 3d\ ^3P_1$–$3s^2\ 3p\ 4f\ ^3F_2$	8.3×10^{-3}	8.6×10^{-3}	8.7×10^{-3}	1.4×10^{-3}	1.22	2.4×10^{11}	–	81.65
20–265	$3s^2\ 3p\ 3d\ ^3P_1$–$3s^2\ 3p\ 4p\ ^3P_0$	8.2×10^{-3}	8.2×10^{-3}	8.2×10^{-3}	8.9×10^{-4}	3.5×10^{-2}	2.1×10^{10}	–	102.91
23–409	$3s^2\ 3p\ 3d\ ^3D_1$–$3s^2\ 3p\ 4f\ ^3F_2$	6.0×10^{-3}	6.3×10^{-3}	6.3×10^{-3}	1.0×10^{-3}	0.91	1.7×10^{11}	–	82.43
1–341	$3s^2\ 3p^2\ ^3P_0$–$3s^2\ 3p\ 4d\ ^3D_1$	5.3×10^{-3}	6.3×10^{-3}	6.6×10^{-3}	1.1×10^{-3}	0.38	2.1×10^{11}	62.353	61.74 (–0.6)
3–210	$3s^2\ 3p^2\ ^3P_2$–$3s^2\ 3p\ 4s\ ^3P_1$	2.9×10^{-3}	4.5×10^{-3}	4.6×10^{-3}	1.8×10^{-3}	0.19	7.3×10^{10}	75.892	75.05 (–0.8)
11–331	$3s\ 3p^3\ ^3P_1$–$3s\ 3p^2\ 4s\ ^3P_0$	3.6×10^{-3}	3.6×10^{-3}	3.6×10^{-3}	3.5×10^{-4}	2.9×10^{-2}	3.1×10^{10}	–	78.31
16–259	$3s^2\ 3p\ 3d\ ^3F_3$–$3s^2\ 3p\ 4p\ ^3D_2$	2.8×10^{-3}	3.1×10^{-3}	3.3×10^{-3}	1.9×10^{-3}	0.28	3.8×10^{10}	–	97.82
2–341	$3s^2\ 3p^2\ ^3P_1$–$3s^2\ 3p\ 4d\ ^3D_1$	2.2×10^{-3}	2.6×10^{-3}	2.7×10^{-3}	4.5×10^{-4}	0.16	8.9×10^{10}	62.717	62.08 (–0.6)
3–344	$3s^2\ 3p^2\ ^3P_2$–$3s^2\ 3p\ 4d\ ^3D_3$	2.1×10^{-3}	2.6×10^{-3}	3.5×10^{-3}	2.8×10^{-3}	0.94	2.2×10^{11}	62.975	62.33 (–0.6)
1–210	$3s^2\ 3p^2\ ^3P_0$–$3s^2\ 3p\ 4s\ ^3P_1$	1.7×10^{-3}	2.6×10^{-3}	2.7×10^{-3}	1.0×10^{-3}	0.11	4.2×10^{10}	74.838	74.03 (–0.8)
7–409	$3s\ 3p^3\ ^3D_1$–$3s^2\ 3p\ 4f\ ^3F_2$	2.3×10^{-3}	2.4×10^{-3}	2.4×10^{-3}	3.9×10^{-4}	0.25	6.8×10^{10}	–	69.39
14–416	$3s\ 3p^3\ ^3S_1$–$3s\ 3p^2\ 4s\ ^3P_0$	2.3×10^{-3}	2.4×10^{-3}	2.4×10^{-3}	2.9×10^{-4}	7.0×10^{-2}	7.9×10^{10}	–	76.00
20–331	$3s^2\ 3p\ 3d\ ^3P_1$–$3s\ 3p^2\ 4s\ ^3P_0$	2.3×10^{-3}	2.3×10^{-3}	2.3×10^{-3}	2.2×10^{-4}	2.5×10^{-2}	1.9×10^{10}	–	90.55
16–407	$3s^2\ 3p\ 3d\ ^3F_3$–$3s^2\ 3p\ 4f\ ^3G_4$	1.6×10^{-3}	1.8×10^{-3}	1.9×10^{-3}	2.4×10^{-3}	3.65	4.4×10^{11}	78.770	77.92 (–0.8)
8–334	$3s\ 3p^3\ ^3D_2$–$3s\ 3p^2\ 4s\ ^3P_1$	7.9×10^{-4}	1.3×10^{-3}	1.3×10^{-3}	3.4×10^{-3}	0.29	1.1×10^{11}	–	75.42
3–218	$3s^2\ 3p^2\ ^3P_2$–$3s^2\ 3p\ 4s\ ^3P_2$	3.5×10^{-4}	1.3×10^{-3}	1.4×10^{-3}	3.5×10^{-3}	0.39	9.0×10^{10}	–	74.25
9–343	$3s\ 3p^3\ ^3D_3$–$3s\ 3p^2\ 4s\ ^3P_2$	6.0×10^{-4}	1.1×10^{-3}	1.1×10^{-3}	5.3×10^{-3}	0.46	1.0×10^{11}	–	75.10
9–272	$3s\ 3p^3\ ^3D_3$–$3s^2\ 3p\ 4p\ ^3P_2$	5.7×10^{-4}	9.6×10^{-4}	1.0×10^{-3}	3.6×10^{-3}	9.7×10^{-2}	1.8×10^{10}	–	83.51
18–267	$3s^2\ 3p\ 3d\ ^3F_4$–$3s^2\ 3p\ 4p\ ^3D_3$	3.3×10^{-4}	7.7×10^{-4}	8.6×10^{-4}	2.7×10^{-3}	0.42	4.0×10^{10}	–	97.54
25–272	$3s^2\ 3p\ 3d\ ^3D_3$–$3s^2\ 3p\ 4p\ ^3P_2$	4.3×10^{-4}	7.3×10^{-4}	7.6×10^{-4}	2.7×10^{-3}	0.11	1.4×10^{10}	–	103.23
26–428	$3s^2\ 3p\ 3d\ ^1F_3$–$3s^2\ 3p\ 4f\ ^1G_4$	3.7×10^{-4}	4.6×10^{-4}	4.9×10^{-4}	5.9×10^{-3}	5.15	5.4×10^{11}	84.275	83.57 (–0.7)
12–343	$3s\ 3p^3\ ^3P_2$–$3s\ 3p^2\ 4s\ ^3P_2$	2.4×10^{-4}	4.3×10^{-4}	4.4×10^{-4}	2.1×10^{-3}	0.20	4.2×10^{10}	–	77.51
25–417	$3s^2\ 3p\ 3d\ ^3D_3$–$3s^2\ 3p\ 4f\ ^3F_4$	2.6×10^{-4}	4.0×10^{-4}	4.3×10^{-4}	2.2×10^{-3}	2.81	3.0×10^{11}	–	81.92
26–282	$3s^2\ 3p\ 3d\ ^1F_3$–$3s^2\ 3p\ 4p\ ^1D_2$	1.4×10^{-4}	3.7×10^{-4}	4.0×10^{-4}	5.5×10^{-3}	0.19	2.2×10^{10}	107.384	106.78 (–0.6)
1–20	$3s^2\ 3p^2\ ^3P_0$–$3s^2\ 3p\ 3d\ ^3P_1$	1.0	1.0	1.0	0.12	0.84	4.5×10^{10}	202.044(1)	198.96 (–3.1)

Notes. The lines are displayed in decreasing order of intensity (photons) Int = $N_j A_{ji}/N_e$ relative to the strongest 1–20 line (in the EUV). The intensities were calculated at log T_e [K] = 6.25. Columns 3, 4, 5 show the relative intensities calculated at log N_e [cm^{-3}] = 8 with the DW4, RM4, and RM4+DW6 ion models. Column 6 shows the values at log N_e [cm^{-3}] = 12 from the RM4 ion model. Columns 7, 8 show the gf and A values calculated in this work. The last two columns show the wavelengths corresponding to the experimental and target energies. Values in parenthesis list the corresponding wavelength difference.

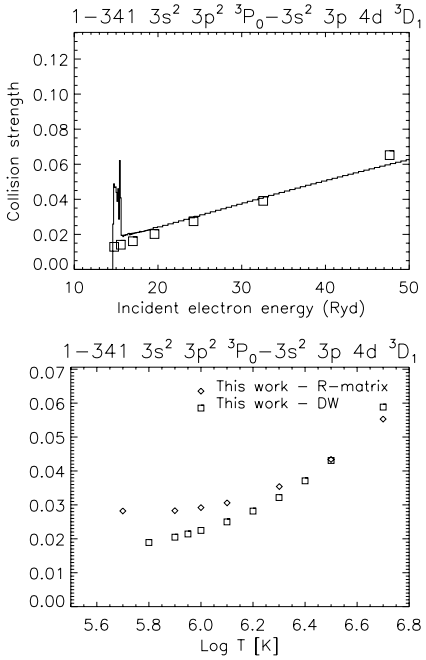

Fig. 5. Same as Fig. 3, for the 1–341 transition.

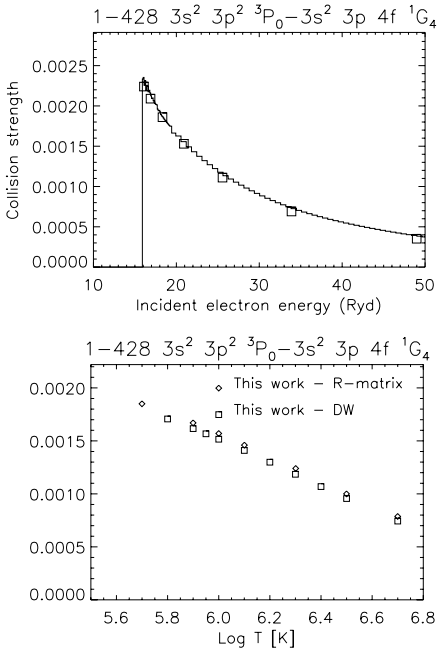

Fig. 6. Same as Fig. 3, for the 1–428 transition.

However, as we expected, we find significant resonance contributions for transitions to a number of levels, in particular to the $3s^2\ 3p\ 4s$ ones. One of the strongest lines from these levels is the 1–210 $3s^2\ 3p^2\ ^3P_0$–$3s^2\ 3p\ 4s\ ^3P_1$ line. Within the RM4 model, the upper level is mainly populated by direct excitation (78%), mostly from the ground state (73%), however

significant contribution from radiative decays is present (22%). Figure 3 shows the collision strength for the 1–210 transition, showing a strong enhancement due to resonances. The intensity of the line is increased by 50%.

The $3s^2$ 3p 4p levels are also affected by resonance enhancements. Figure 4 shows as an example the collision strength for the 1–282 transition. Level 282 ($3s^2$ 3p 4p $^1D_2$) is populated by 95% via direct excitations, mostly (67%) from the ground state, but then its main radiative decay is to level 26. The RM4 model produces a large increase (factor of 2.6) in the intensity of the 26–282 line, compared to the DW4 model.

The other $n = 4$ levels are generally less affected by resonance enhancements and radiative decays. Figure 5 shows the collision strength for the 1–341 transition. Level 341 ($3s^2$ 3p 4d $^3D_1$) is mainly (97%) populated via direct excitation from the ground state, and then mainly decays to the same state via a previously identified transition. The difference in terms of line intensity between the RM4 and DW4 is only 19%. Figure 6 shows the collision strength for the 1–428 transition. Level 428 ($3s^2$ 3p 4f $^1G_4$) is populated by direct excitation from the ground state (66%) and the $3s^2$ $3p^2$ $^3P_2$ (18%). Its main decay is to level 26 ($3s^2$ 3p 3d $^1F_3$). The RM4 model predicts an intensity 24% higher than that one of the DW4 case.

We predict that the strongest soft X-ray line is the 7–331 3s $3p^3$ $^3D_1$–3s $3p^2$ 4s $^3P_0$ transition. Level 331 is excited from the ground state, but the collision strengths does not have any resonance enhancement. Indeed both the RM4 and the DW4 models predict the same intensity for the 7–331 line.

4.4. DW calculations for the n = 5, 6 levels

To estimate the effects of further cascading from even higher levels, we built a new target by adding the following configurations to the R-matrix $n = 4$ one (RM4): $3s^2$ 3p $5l$, 3s $3p^2$ $5l$, $3p^3$ $5l$, $3s^2$ 3p $6l$, 3s $3p^2$ $6l$, and $3p^3$ $6l$ (l = s, p, d, f, g). We kept the scaling parameters for the $n = 4$ the same, and obtained those for the $n = 5, 6$, which are listed in Table 1. This was done to try and keep similar energies (and ordering of the levels) for the $n = 4$ levels.

The total target comprises 65 configurations, 1344 *LS* terms and 3066 fine-structure levels. We then used the DW code to calculate the excitation rates up to all of these levels, but just from the lowest 27 arising from the $3s^2$ $3p^2$, 3s $3p^3$, and $3s^2$ 3p 3d configurations. This number was chosen to include all possible metastable levels which may contribute to the populations of the remaining levels.

We then calculated separately the radiative rates between all the 3066 levels, and matched the ordering of this calculation with that of the 749-levels RM4. We then merged the rates and A-values from RM4 with those from this DW run, and built an ion model, which we indicate as RM4+DW6. The relative intensities of the main soft X-ray lines as obtained with the RM4+DW6 model are also shown in Table 4.

Cascading generally increases line intensities by small amounts (less than 10%), however some transitions are more affected, for example the 3–344 $3s^2$ $3p^2$ $^3P_2$–$3s^2$ 3p 4d $^3D_3$ line intensity is increased by 35%.

5. Conclusions

We have presented the results of R-matrix calculations for the $n = 4$ levels in Fe XIII. We found the same situation that we described for Fe X, and which was also present in Fe XII, i.e. there are large resonance enhancements of the excitation rates to levels of some $n = 4$ configurations, while excitation by cascading from higher levels is a less significant effect. As found in Fe X and Fe XII, the resonance enhancements are principally due to other configurations with $n = 4$. Generally, cascading from the $n = 5, 6$ levels increases line intensities by small amounts, of the order of 10%.

We found that a large number of transitions which we predict to be strong arise from levels which are not known experimentally and therefore have no known wavelength. In particular, the decays from the the experimentally unidentified 3s $3p^2$ 4s levels are predicted to be stronger than those from $3s^2$ 3p 4s whose wavelengths are well established. The identifications of these levels will be discussed in a separate paper.

Acknowledgements. G.D.Z. acknowledges the support from STFC via the Advanced Fellowship programme. We acknowledge support from STFC for the UK APAP network. B.C. Fawcett is thanked for his contribution in rescuing some of his original plates, and for the continuous encouragement over the years.

References

Badnell, N. R. 1997, J. Phys. B Atom. Mol. Phys., 30, 1
Badnell, N. R. 2011, Comput. Phys. Comm., 182, 1528
Badnell, N. R., & Griffin, D. C. 2001, J. Phys. B Atom. Mol. Phys., 34, 681
Behring, W. E., Cohen, L., Doschek, G. A., & Feldman, U. 1976, ApJ, 203, 521
Berrington, K. A., Eissner, W. B., & Norrington, P. H. 1995, Comput. Phys. Comm., 92, 290
Brinkman, A. C., Gunsing, C. J. T., Kaastra, J. S., et al. 2000, ApJ, 530, L111
Burgess, A. 1974, J. Phys. B Atom. Mol. Phys., 7, L364
Burgess, A., & Tully, J. A. 1992, A&A, 254, 436
Burgess, A., Chidichimo, M. C., & Tully, J. A. 1997, J. Phys. B Atom. Mol. Phys., 30, 33
Chidichimo, M. C., Badnell, N. R., & Tully, J. A. 2003, A&A, 401, 1177
Del Zanna, G. 2011, A&A, 533, A12
Del Zanna, G. 2012, A&A, 537, A38
Del Zanna, G., & Mason, H. E. 2005, A&A, 433, 731
Del Zanna, G., Storey, P. J., Badnell, N. R., & Mason, H. E. 2012a, A&A, 541, A90
Del Zanna, G., Storey, P. J., Badnell, N. R., & Mason, H. E. 2012b, A&A, submitted
Fawcett, B. C., Peacock, N. J., & Cowan, R. D. 1968, J. Phys. B Atom. Mol. Phys., 1, 295
Fawcett, B. C., Kononov, E. Y., Hayes, R. W., & Cowan, R. D. 1972, J. Phys. B Atom. Mol. Phys., 5, 1255
Griffin, D. C., Badnell, N. R., & Pindzola, M. S. 1998, J. Phys. B Atom. Mol. Phys., 31, 3713
Hummer, D. G., Berrington, K. A., Eissner, W., et al. 1993, A&A, 279, 298
Kastner, S. O., Swartz, M., Bhatia, A. K., & Lapides, J. 1978, J. Opt. Soc. Am., 68, 1558
Lemen, J. R., Title, A. M., Akin, D. J., et al. 2012, Sol. Phys., 275, 17
Manson, J. E. 1972, Sol. Phys., 27, 107
O'Dwyer, B., Del Zanna, G., Badnell, N. R., Mason, H. E., & Storey, P. J. 2012, A&A, 537, A22
Storey, P. J., & Zeippen, C. J. 2010, A&A, 511, A78 (SZ10)
Storey, P. J., Del Zanna, G., Mason, H. E., & Zeippen, C. 2005, A&A, 433, 717
Vilkas, M. J., & Ishikawa, Y. 2004, Phys. Rev. A, 69, 062503
Woods, T. N., Eparvier, F. G., Hock, R., et al. 2012, Sol. Phys., 275, 115